© Sagdullaeva S.A., Koniaeva A.D., Varakuta E.Yu, Bolbasov E.N., Chernova U.V., Kukartseva O.V., 2026

DOI: 10.31088/CEM2026.15.5.45-55

Morphological characteristics of the microcirculatory network in regenerating purulent wounds with piezoelectric polymer smart membranes

S.A. Sagdullaeva[1], A.D. Koniaeva[1], E.Yu. Varakuta[1], E.N. Bolbasov[2], U.V. Chernova[2], O.V. Kukartseva[2]

[1] Siberian State Medical University, Tomsk, Russia
[2] National Research Tomsk Polytechnic University, Tomsk, Russia

Abstract. *Introduction.* Purulent oral wounds are associated with marked microcirculatory disturbances that impair tissue regeneration. Therefore, wound coverings that restore the vascular component are of particular interest. This study evaluated morphological changes in the microcirculatory network during regeneration of purulent oral wounds treated with antibacterial piezoelectric polymer smart membranes.
Materials and methods. Sixty Wistar rats were divided into four groups (n=15 each): untreated purulent wounds, smart membranes without an antibacterial layer, smart membranes with an antibacterial layer, and intact controls. On days 3, 7, and 14, we assessed the Kernohan index, pericapillary diffusion index, arteriolar-venular ratio, numerical density of altered arterioles and venules, VEGF expression, and endothelial ultrastructure.
Results. Early inflammation-associated microcirculatory disturbances occurred in all wound groups. Membrane-treated groups showed partial microcirculatory recovery by day 7. On day 14, VEGF expression in groups 2 and 3 was 2.8- and 5.8-fold higher, respectively than in the untreated group ($p=0.0287$ and $p=0.0001$). In group 3, most parameters approached intact-control values. In the untreated group, however, the Kernohan index remained 1.5-fold higher ($p=0.0027$) and the arteriolar-venular ratio 1.3-fold lower ($p=0.0035$) than in intact controls, with numerous altered arterioles and venules.
Conclusion. Antibacterial piezoelectric polymer smart membranes promoted angiogenic activity and accelerated restoration of the microcirculatory network in purulent oral wounds, with near-normalization of most parameters by day 14.

Keywords: purulent wound, smart materials, regeneration, piezoelectrics, microcirculation

Corresponding author: Anastasiia D. Koniaeva. E-mail: asyakonya95@gmail.com

For citation: Sagdullaeva S.A., Koniaeva A.D., Varakuta E.Yu, Bolbasov E.N., Chernova U.V., Kukartseva O.V. Morphological characteristics of the microcirculatory network in regenerating purulent wounds with piezoelectric polymer smart membranes. Clin. exp. morphology. 2026;15(5):45–55. DOI: 10.31088/CEM2026.15.5.45-55.

This article is distributed under the terms of the Creative Commons Attribution-NonCommercial 4.0 International (CC BY-NC 4.0).

Funding. The comprehensive morphological study was carried out with the financial support of the Russian Science Foundation within the framework of scientific project No. 23-25-00346. The production of antibacterial smart coatings was completed at Tomsk Polytechnic University with the support of Priority-2030-IZ-025-202-2024 project.

Received 19.03.2026. **Received in revised form** 13.04.2026. **Accepted** 14.05.2026.

УДК: 616-018

Морфологическая характеристика микроциркуляторного русла при регенерации гнойной раны с использованием антибактериальных пьезоэлектрических полимерных смарт-мембран

С.А. Сагдуллаева[1], А.Д. Коняева[1], Е.Ю. Варакута[1], Е.Н. Больбасов[2], У.В. Чернова[2], О.В. Кукарцева[2]

[1] ФГБОУ ВО Сибирский государственный медицинский университет Минздрава России, Томск, Россия
[2] ФГАОУ ВО Национальный исследовательский Томский политехнический университет, Томск, Россия

Резюме. *Введение.* Гнойные раны ротовой полости характеризуются выраженным нарушением микроциркуляции, являющимся ключевым звеном патогенеза в ходе регенерации. Актуальность приобретает разработка покрытий, благоприятно влияющих на восстановление сосудистого компонента. Целью исследования явилось проведение морфологической оценки состояния микроциркуляции в зоне

регенерации гнойной раны слизистой оболочки полости рта при использовании антибактериальных пьезоэлектрических полимерных смарт-мембран.

Материалы и методы. Исследование проводилось на 60 крысах линии Вистар, разделенных на группы: 1-я (n=15) – регенерация гнойной раны без покрытия, 2-я (n=15) – применение смарт-мембраны без антибактериального напыления, 3-я (n=15) – применение смарт-мембраны с антибактериальным напылением, 4-я (n=15) – интактные животные. Индексы Керногана и перикапиллярной диффузии, артериоло-венулярное взаимоотношение, численная плотность измененных артериол и венул, ультраструктурные изменения эндотелиоцитов, экспрессия VEGF исследовались на 3-и, 7-е и 14-е сутки эксперимента.

Результаты. В ранние сроки в экспериментальных группах выявлялись выраженные воспалительно ассоциированные нарушения микроциркуляции. В группах с раневым покрытием частичное восстановление микроциркуляции отмечалось уже на 7-е сутки исследования. Значимое повышение экспрессии VEGF, отражающее ангиогенез, отмечалось на 14-е сутки во 2-й и 3-й группах и было в 2,8 и 5,8 раза достоверно выше, чем в 1-й группе (p=0,0287; p=0,0001). Остальные показатели в 3-й группе на 14-е сутки восстанавливались до значений у интактных особей. В 1-й группе индекс Керногана был в 1,5 раза достоверно больше (p=0,0027), а артериоло-венулярное взаимоотношение в 1,3 раза значимо ниже (p=0,0035), чем в группе контроля, в большом количестве визуализировались измененные артериолы и венулы.

Заключение. Применение антибактериальных пьезоэлектрических полимерных смарт-мембран обеспечивало восстановление микроциркуляторного русла за счет нормализации эндотелиальной функции, гемодинамики и процессов ангиогенеза. Выявленные изменения свидетельствовали о формировании функционально зрелой сосудистой сети в более короткие сроки по сравнению с другими экспериментальными группами.

Ключевые слова: гнойная рана, смарт-материалы, регенерация, пьезоэлектрики, микроциркуляция

Для корреспонденции: Анастасия Денисовна Коняева. E-mail: asyakonya95@gmail.com

Для цитирования: Сагдуллаева С.А., Коняева А.Д., Варакута Е.Ю., Больбасов Е.Н., Чернова У.В., Кукарцева О.В. Морфологическая характеристика микроциркуляторного русла при регенерации гнойной раны с использованием антибактериальных пьезоэлектрических полимерных смарт-мембран. Клин. эксп. морфология. 2026;15(5):45–55. DOI: 10.31088/CEM2026.15.5.45-55.

Эта статья распространяется на условиях международной лицензии Creative Commons Attribution-NonCommercial 4.0 International (CC BY-NC 4.0).

Финансирование. Комплексное морфологическое исследование проведено при финансовой поддержке Российского научного фонда в рамках научного проекта № 23-25-00346. Изготовление антибактериальных смарт-покрытий выполнено в Томском политехническом университете при поддержке проекта «Приоритет-2030-ИЗ-025-202-2024».

Статья поступила 19.03.2026. **Получена после рецензирования** 13.04.2026. **Принята в печать** 14.05.2026.

Introduction

Treating purulent wounds remains a significant challenge in surgical dentistry due to their high incidence, tendency for chronic inflammation, and the development of severe infectious and deformational complications [1].

Modern approaches to managing purulent wounds are increasingly focused not only on suppressing microbial contamination but also on creating favorable local environment for tissue regeneration. In this context, the development of wound dressings that combine antibacterial properties and modulate local tissue responses is of particular interest [2].

Polymers with piezoelectric properties belong to smart materials capable of interacting with the biological environment when biointegrating [3]. Available data suggest that their use is associated with diminished postoperative scarring and may promote more effective repair of purulent wounds that usually heal by secondary intention, where coarse fibrous connective tissue is typically formed [4]. In addition, several studies have investigated the influence of piezoelectric membranes on the healing of aseptic skin wounds and full 3D skin reconstruction [5].

At the same time, antibacterial coatings that provide prolonged release of antimicrobial agents directly at the wound site allow to reduce the bacterial load and minimize the systemic effects of antibiotic therapy, which may contribute to a more favorable course of wound healing [6].

A polymer-based piezoelectric membrane was created at the Shared Access Additive Technology Center of the National Research Tomsk Polytechnic University and proved to be effective in the treatment of non-purulent wounds of the oral mucosa [7]. A distinctive feature of the membrane is that it is able to modify its surface with various pharmaceutical agents, including antibacterial compounds. Therefore, the present study examines the local effects of piezoelectric polymer smart membranes modified with an antibacterial agent [8] in purulent wound regeneration.

This paper focuses on the results related to the restoration of the microcirculatory bed, since microcirculato-

ry disturbances in the area of injury are considered a key pathogenic factor that impedes adequate tissue regeneration and contributes to persistent inflammation. In purulent inflammation, the structural organization of the microvascular network undergoes pronounced alterations, including endothelial dysfunction, vascular stasis, increased vascular permeability, and impaired angiogenesis. These changes lead to tissue hypoxia, delayed reparative processes, and the formation of morphologically and functionally inferior connective tissue.

Most studies on wound dressings concentrate primarily on clinical outcomes and the dynamics of wound healing, whereas the morphological changes occurring in the microcirculatory bed within the regeneration zone remain insufficiently investigated. However, the structural organization of the vascular network largely determines the quality of the newly formed tissue and the functional outcome of wound healing. The study of microvascular network, pathological alterations, density, and the degree of maturity of microvessels makes it possible to gain deeper insight into the mechanisms underlying the influence of local antibacterial therapy on reparative processes and to substantiate the prospects for the use of modern wound dressings as part of a pathogenetically oriented treatment of purulent wounds [9].

Thus, the aim of this research was to perform a morphological assessment of microcirculatory vessel changes in healing purulent oral mucosa wounds following the application of antibacterial piezoelectric polymer smart membranes.

Materials and methods

We designed the experiment as a comparative exploratory study in order to investigate the morphological aspects of purulent wound regeneration of the oral mucosa following the application of piezoelectric polymer smart membranes with and without antibacterial properties.

Experimental wound dressing samples were designed and fabricated at the Shared Access Additive Technology Center of National Research Tomsk Polytechnic University from powder of vinylidene fluoride-tetrafluoroethylene copolymer (VDF-TeFE, Galopolymer, Russia) using electrospinning technique. Two types of polymer piezoelectric smart membranes were developed: piezoelectric polymer membranes and piezoelectric polymer membranes containing an antibacterial agent.

We developed the smart covering membrane modified with an antibiotic agent in order to evaluate the ability of the piezoelectric wound dressing to provide a prolonged local antibacterial effect. Vancomycin served as the model antibacterial agent because of its pronounced activity against Gram-positive microorganisms, particularly *Staphylococcus aureus*, a strain of which was used to establish a model of a purulent wound. Moreover, vancomycin possesses a well-characterized mechanism of action, predictable antibacterial efficacy, and high chemical stability [10].

The study was conducted at the Siberian State Medical University, and the experimental protocol was approved by the local Institutional Animal Care and Use Committee (IACUC, protocol No. 1 dated December 16, 2022). All animal procedures were performed in accordance with Directive 2010/63/EU of the European Parliament and of the Council of 22 September 2010 on the protection of animals used for scientific purposes.

The experiment included 60 three-month-old male Wistar rats weighing 250–300 g, provided by Goldberg Research Institute of Pharmacology and Regenerative Medicine (Tomsk, Russia). The animals were housed under standard vivarium conditions in accordance with the sanitary and epidemiological requirements for experimental biological facilities established by 2.2.1.3218-14 "On Sanitary and Epidemiological Requirements for the Design, Equipment, and Maintenance of Experimental Biological Clinics (Vivariums)," approved by the Russian Federation Chief State Sanitary Doctor Resolution No. 51 of August 29, 2014. Prior to the experiment, all animals underwent a two-week acclimatization period.

We randomly assigned the animals to four equal groups using block randomization. Groups 1–3 were experimental: group 1 included animals in which the wound defect was not covered with a piezoelectric polymer smart membrane; group 2, those in which it was covered with a non-modified piezoelectric polymer smart membrane; and group 3, those in which the defect was covered with antibacterial piezoelectric polymer smart membrane. Group 4 served as the control group and comprised animals with intact oral mucosa.

All surgical procedures were performed in accordance with the Refinement principle of the 3Rs. Premedication was administered using atropine sulfate (Dalchimpharm, Russia) at a dose of 0.04 mg/kg subcutaneously 30 minutes prior to induction of anesthesia with Zoletil-100 (Virbac, France) at a dose of 10 mg/kg. Criteria for animal removal, followed by euthanasia, included deterioration of general condition manifested by lethargy, apathy, refusal to eat, sleep disturbances, fever, or premature death. No animals were excluded from the study.

The experimental model of a purulent wound was created using the following procedure. In groups 1–3, a mucosal flap measuring 5 × 2 mm was excised from the buccal region using a standardized template. Subsequently, the wound margins and bottom were mechanically crushed with a Kocher clamp for 4 minutes and infected by applying a suspension of a 24-hour culture of *Staphylococcus aureus* at a concentration of 1×10^9 microbial bodies per 1 mL of physiological saline to a foam pellet (Pele Tim No. 1, d=4 mm); the total volume of the microbial suspension applied was 0.4 mL. After inoculation, we tightly sutured the wound edges with the foam pellet using PGA 4/0 suture material.

On day 3, we removed the sutures, extracted the foam pellet, and irrigated the wound with 1 mL of physiological saline. Following this, in groups 2 and 3, a smart membrane

was fixed along the wound margins using simple interrupted sutures with an atraumatic needle.

Five animals from each group were euthanized on days 3, 7, and 14 by exposure to CO_2 in a chamber (ZOONLAB, Germany). The selection of these time points was based on current concepts regarding the pathomorphological phases of wound healing [11]. After euthanasia, tissue samples from the wound area, including surrounding tissues with a 5-mm peripheral margin, were harvested for autopsy examination.

The samples were fixed in 10% neutral buffered formalin (Biovitrum, Russia), rinsed in running water, dehydrated in graded alcohols and isopropanol (Biovitrum, Russia), and embedded in paraffin (Biovitrum, Russia). Then, we prepared histological sections 5 μm thick using a sliding microtome Leica SM 2010R (Leica, Germany) and stained with hematoxylin and eosin (Abris+, Russia).

Histological specimens were examined using a bright-field microscope (Axioskop 40, Carl Zeiss, Germany; 10×, 40×, and 90× objective lenses; 10× eyepiece). In each group, we analyzed a total of 100 fields of view and assessed the following parameters: numerical density of altered arterioles and venules (with stasis, erythrocyte aggregation, and thrombosis) per 1 mm² of the section; the Kernogan index (an indicator of arteriolar conductance), calculated as the ratio of the arterial wall thickness to the radius of the vascular lumen; the pericapillary diffusion index (the area of tissue supplied by a single capillary), calculated as the ratio of the mean capillary diameter to the specific capillary area; and the arteriolar-venular ratio.

Image processing and morphometric analysis were performed using AxioVision Viewer 4.8 (Carl Zeiss, Germany) and ImageJ 1.52u (National Institutes of Health, USA) [12].

Specimens for electron microscopy were prepared by fixation in 2.5% glutaraldehyde in 0.2M cacodylate buffer (1:9), followed by postfixation in 1% OsO_4 at 4°C for 4 hours. After dehydration, the samples were embedded in an epoxy resin (Epon). Semi-thin sections were stained with Azure II, whereas ultrathin sections were contrasted with uranyl acetate and lead citrate. The ultrastructure of endothelial cells of the microcirculatory vessels was then examined using a JEOL JEM-1400 CX transmission electron microscope (JEOL, Japan).

For immunohistochemical analysis, serial paraffin sections 4–6 μm thick were prepared and stained using rabbit recombinant polyclonal IgG antibodies against vascular endothelial growth factor A (VEGF-A; Abcam, USA). The slides were scanned using a Pannoramic MIDI III digital slide scanner (3DHISTECH, Hungary).

Subsequently, the number of VEGF-expressing cells per 1,000 cells was quantified using Pannoramic Diagnostic Scanner Software 2.1 (3DHISTECH, Hungary). Ten annotation areas were selected on each specimen, with a total area of 1 mm² analyzed per slide.

Statistical analysis was performed using Statistica 10.0 software (StatSoft Inc., USA). The distribution of variables was assessed using the Kolmogorov–Smirnov test. We analyzed data with descriptive and nonparametric statistical methods and presented the studied parameters as the median and quartiles, M (Q1; Q3).

Comparisons between independent groups were performed using the Kruskal–Wallis test with Bonferroni correction, whereas those of related samples were carried out using the Wilcoxon test. Differences were considered statistically significant at $p<0.05$.

Results

On day 3, all experimental groups exhibited structural abnormalities within the microcirculatory network at wound periphery, including arterioles, venules, and capillaries. These vessels were characterized by perivascular edema, vascular stasis, and erythrocyte aggregation (Fig. 1 A, B).

Intergroup analysis revealed no significant differences in the numerical density of altered arterioles per 1 mm² of section, which was 11.93 (10.89; 12.95; p=0.079). For altered venules, the numerical density per 1 mm² did not significantly differ between groups 1 and 2, whereas it was 2.15-fold lower in group 3 than in groups 1 and 2 (p=0.023).

Capillary numerical density was 1.2 times lower in groups 1 and 2 than in group 3 and the control group [p=0.036] (Table).

Reduced arteriolar conductance was observed in all experimental groups, as evidenced by a marked elevation of the Kernogan index. Compared with the control group, the index was 3.5, 2.4, and 1.9 times higher in groups 1, 2, and 3, respectively (p=0.0003, p=0.0183, p=0.0287). These observations indicate increased vascular wall tone and arteriolar lumen constriction. Furthermore, in group 3, it was 1.9-fold lower than in group 1 [p=0.035] (Table).

A three-fold reduction in the arteriolar-venular ratio was observed across all experimental groups compared with the control group [p=0.027] (Table), suggesting a pronounced inflow–outflow imbalance.

Similarly, the pericapillary diffusion index was significantly reduced across all experimental groups, falling 1.6-fold below control levels [p=0.039] (Table), indicating ongoing shortening of the diffusion distance and functional capillary immaturity.

Active angiogenesis was reflected by a significant increase in cellular VEGF expression. The highest expression levels were observed in groups 2 and 3, which were 17.4 and 2.4 times higher, respectively, than those in the control group and group 1 [p=0.015 and p=0.033, respectively] (Fig. 2 A, B; Table).

At the ultrastructural level, all experimental groups exhibited characteristic endothelial layer thinning, cytoplasmic vacuolization of endothelial cells, and disorganization of intercellular junctions. Micropinocytotic vesicles and plasmalemmal protrusions, reflecting active transcapillary exchange, were poorly expressed (Fig. 3 A).

On day 7, groups 2 and 3 demonstrated a tendency toward restoration of microcirculation in the wound area (Fig. 1 C).

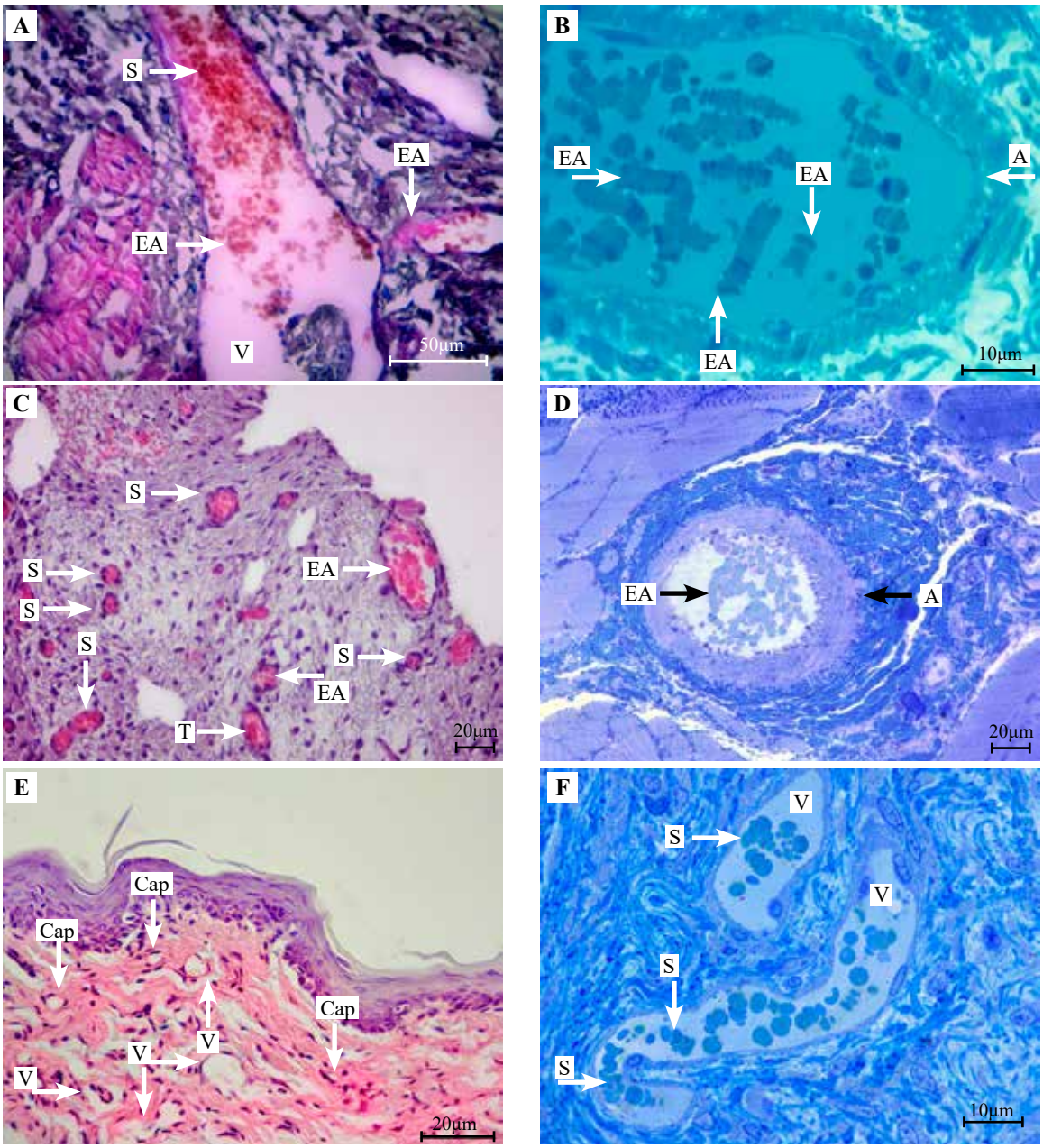


Fig. 1. Microscopic changes in the microcirculatory vessels during regeneration of an oral mucosa purulent wound.
A – pathologically changed vessels with signs of perivascular edema characteristic of all experimental groups. Day 3. B – arterial wall thickening and the presence of erythrocyte aggregation characteristic of all experimental groups. Day 3. C – pathologically changed microcirculatory vessels and vessels without signs of erythrocyte aggregation, stasis, and thrombosis. Group 2. Day 7. D – arteriole with a thickened vascular wall and the presence of erythrocyte aggregation in the vascular lumen. Group 1. Day 7. E – restored oral mucosa with vessels without pathological changes. Group 3. Day 14. F – erythrocyte aggregation in the venular lumen. Group 1. Day 14. A, C, E – H&E stain, ×400; B, D, F – Azure II staining, ×1,000
A – arteriole, V – venule, Cap – capillary, EA – erythrocyte aggregation, S – stasis, T – thrombosis

Рис 1. Микроскопические изменения сосудов микроциркуляторного русла при регенерации гнойной раны слизистой оболочки полости рта.
А – патологически измененные сосуды с признаками периваскулярного отека, характерные для всех экспериментальных групп. 3-и сутки исследования. В – утолщение артериальной стенки и наличие сладжа форменных элементов, характерное для всех экспериментальных групп. 3-и сутки. С – патологически измененные сосуды микроциркуляторного русла, а также сосуды без признаков сладжа, стаза и тромбоза. 2-я экспериментальная группа. 7-е сутки. D – артериола с утолщенной сосудистой стенкой и наличием сладжированных форменных элементов в просвете сосуда. 1-я экспериментальная группа. 7-е сутки. Е – восстановленная слизистая оболочка полости рта с сосудами без патологических изменений. 3-я экспериментальная группа. 14-е сутки. F – сладж форменных элементов в просвете венулы. 1-я экспериментальная группа. 14-е сутки исследования. А, С, Е – окрашивание гематоксилином и эозином, ×400; В, D, F – окрашивание азуром II, ×1000
А – артериола, V – венула, Cap – капилляр, EA – агрегация эритроцитов, S – стаз, T – тромбоз

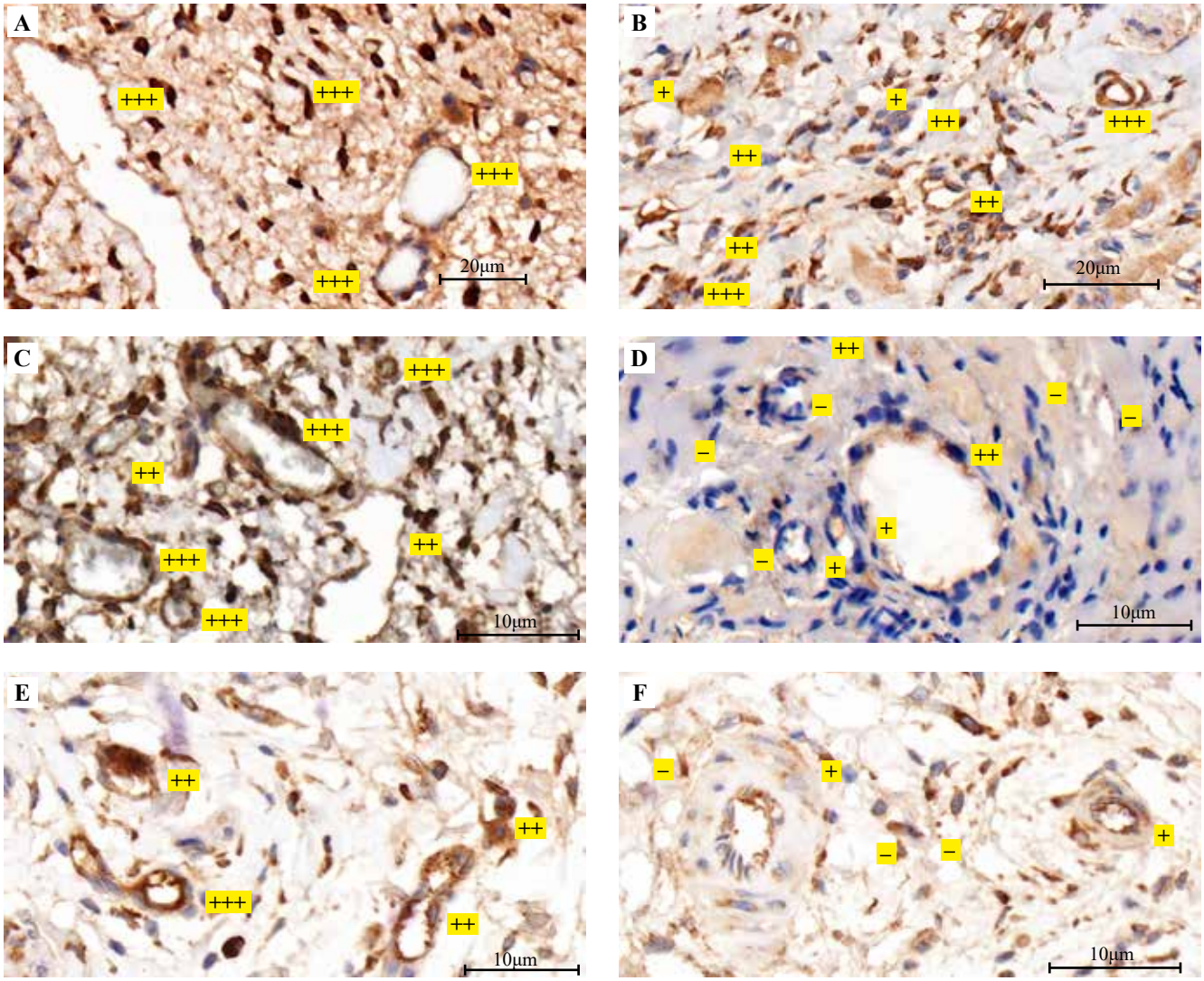


Fig. 2. VEGF expression in the area of purulent wound regeneration.
A – a pattern characteristic of groups 2 and 3. Day 3. B – group 1. Day 3. C – a pattern characteristic of groups 2 and 3. Day 7. D – group 1. Day 7. E – a pattern characteristic of groups 2 and 3. Day 14. F – group 1. Day 14. ×1,000
– – negative expression, + – weak expression, ++ – average expression, +++ – strong expression

Рис 2. Экспрессия VEGF в области регенерации гнойной раны.
A – картина, характерная для 2-й и 3-й экспериментальных групп. 3-и сутки исследования. B – 1-я экспериментальная группа. 3-и сутки исследования. C – картина, характерная для 2-й и 3-й экспериментальных групп. 7-е сутки исследования. D – 1-я экспериментальная группа. 7-е сутки исследования. E – картина, характерная для 2-й и 3-й экспериментальных групп. 14-е сутки исследования. F – 1-я экспериментальная группа. 14-е сутки исследования. ×1000
– – отсутствие экспрессии, + – слабая экспрессия, ++ – средняя экспрессия, +++ – сильная экспрессия

Compared with day 3, a significant decrease in the numerical density of altered arterioles and venules was observed across all experimental groups. In group 3, the reduction in the parameter was substantially greater than in group 1 (3.2- and 2-fold, respectively; p=0.034; p=0.041).

On day 3, groups 2 and 3 showed the arteriolar-venular ratio to be 1.7 times higher than in group 1 [p=0.0005; p=0.0004] (Fig. 1 D), indicating partial correction of inflow–outflow imbalance, and remained significantly lower than control values [p=0.003; p=0.004] (Table).

Compared with day 3, a significant reduction in the Kernogan index was observed in all experimental groups. In group 3, it was 1.8 and 1.4 times lower than in groups 1 and 2, respectively, although control levels were not attained (p=0.027).

The pericapillary diffusion index did not differ significantly between the experimental groups (p=0.077) but remained 1.7-fold below control values [p=0.036] (Table).

VEGF expression in groups 2 and 3 did not change significantly [p=0.066; p=0.059] (Fig. 2 C), whereas

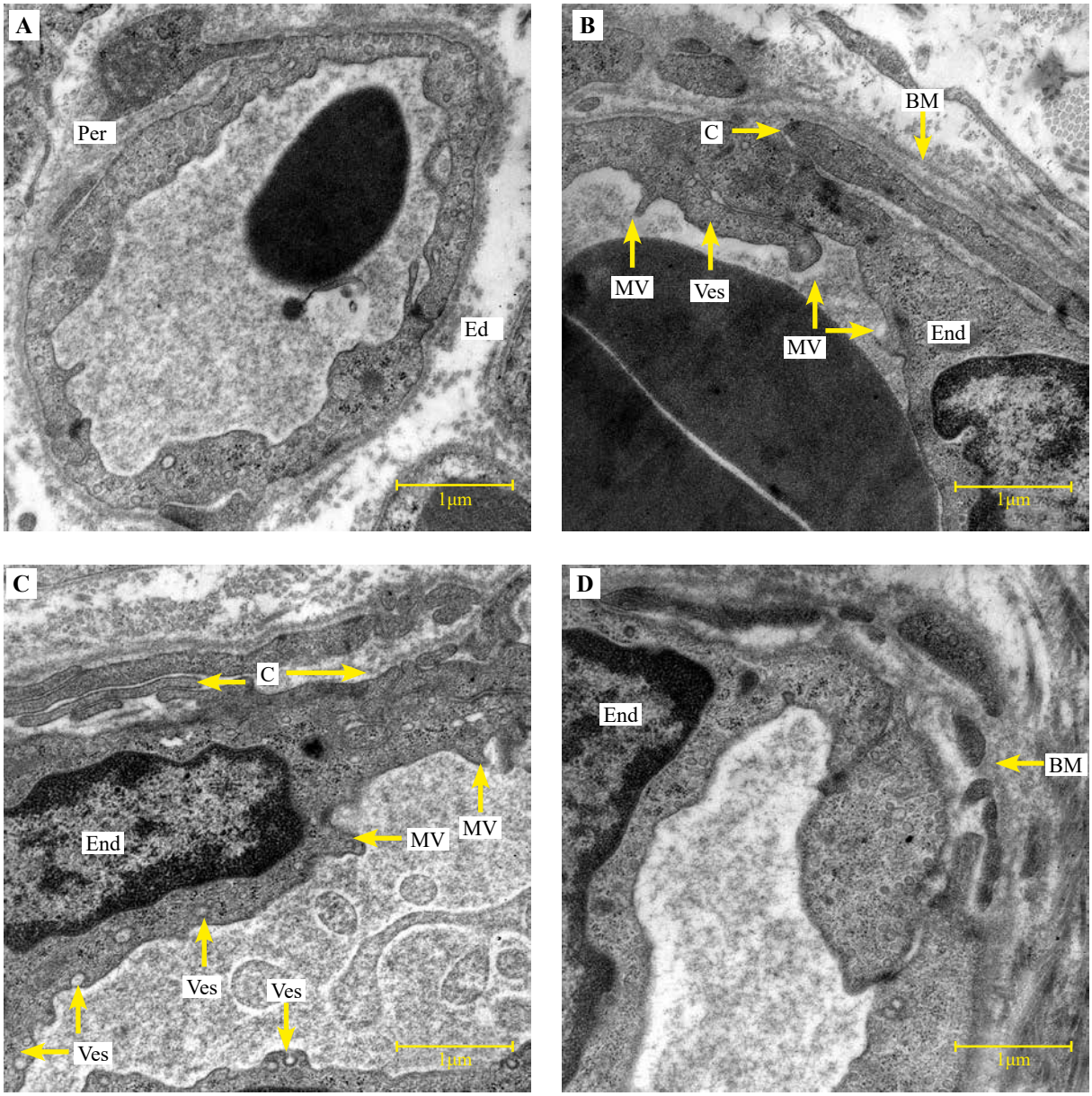


Fig. 3. Ultrastructural changes in the microcirculatory vessels in the area of purulent wound regeneration in the oral mucosa.
A – a vessel with perivascular edema, endothelial layer thinning, and signs of impaired transcapillary exchange. A pattern characteristic of all experimental groups. Day 3. B – gradual restoration of intercellular contacts and transcapillary exchange in the microcirculatory vessels bed in groups 2 and 3. Group 2. Day 7. C – restoration of intercellular contacts and signs of active transcapillary exchange in microcirculatory vessels. Group 3. Day 14. D – disorganization of cellular contacts, impaired transcapillary exchange, and irregularity of the basement membrane in microcirculatory vessels. Group 1. Day 14. ×20,000
End – endothelial cells, Per – pericytes, MV – plasmalemmal protrusions, Ves – micropinocytic vesicles, BM – basement membrane, C – intercellular contacts, Ed – perivascular edema

Рис 3. Ультраструктурные изменения сосудов микроциркуляторного русла в области регенерации гнойной раны слизистой оболочки полости рта.
A – сосуд с периваскулярным отеком и истончением эндотелиального слоя, признаками нарушения транскапиллярного обмена. Картина, характерная для всех экспериментальных групп. 3-и сутки исследования. B – постепенное восстановление межклеточных контактов и транскапиллярного обмена в сосудах микроциркуляторного русла в группах со смарт-мембраной. 2-я экспериментальная группа. 7-е сутки исследования. C – восстановление межклеточных контактов, признаки активного транскапиллярного обмена в сосудах микроциркуляторного русла в группах со смарт-мембраной. 3-я экспериментальная группа. 14-е сутки исследования. D – дезорганизация клеточных контактов, нарушение транскапиллярного обмена, неравномерность базальной мембраны в сосудах микроциркуляторного русла. 1-я экспериментальная группа. 14-е сутки исследования. ×20 000
End – эндотелиоциты, Per – перициты, MV – выросты плазмолеммы, Ves – микропиноцитозные пузырьки, BM – базальная мембрана, C – межклеточные контакты, Ed – периваскулярный отек

Table | Таблица

Morphological indicators of microcirculatory changes in the area of purulent wound healing, Me (Q1–Q3) | Морфологические показатели изменения микроциркуляции в области заживления гнойной раны, Me (Q1–Q3)

	Numerical density of changed arterioles | Численная плотность измененных артериол	Numerical density of changed venules | Численная плотность измененных венул	Numerical density of capillaries | Численная плотность капилляров	Arteriolar-venular ratio | Артериоло-венулярное взаимоотношение	Kernogan index | Индекс Керногана	Pericapillary diffusion index | Индекс перикапиллярной диффузии	VEGF, %
Control | Контроль	–	–	192.7 (188.9; 197.1)	0.72 (0.68; 0.75)	0.39 (0.35; 0.43)	7.8 (7.4; 8.3)	1.5 (1.3; 2.1)
Day 3 | 3-и сутки							
Group 1 | 1-я группа	11.93 (10.89; 12.95)*	24.22 (22.34; 26.78)*&	161.48 (152.52; 169.52)*	0.22 (0.20; 0.23)*	1.38 (1.27; 1.53)*&	5.3 (5.0; 45.5)*	11.0 (10.2; 11.5)*#&
Group 2 | 2-я группа	9.33 (8.88; 10.05)*	19.49 (17.97; 21.82)*	167.8 (159.54; 177.37)*	0.24 (0.24; 0.29)*	0.96 (0.85; 1.10)*	5.4 (5.1; 5.5)*	25.6 (23.4; 26.8)*
Group 3 | 3-я группа	11.02 (10.66; 12.48)*	11.02 (10.04; 12.53)*	174.8 (166.57; 176.24)	0.27 (0.24; 0.30)*	0.74 (0.64; 0.81)*	4.8 (4.1; 5.3)*	26.2 (16.9; 27.9)*
Day 7 | 7-е сутки							
Group 1 | 1-я группа	29.6 (21.7; 32.8)*&	27.2 (21.5; 32.9)*&	216.6 (213.5; 218.8)	0.3 (0.2; 0.3)*#&	0.9 (0.8; 1.0)*&	4.1 (4.0; 4.4)*	4.5 (2.8; 5.1)*#&
Group 2 | 2-я группа	18.1 (17.8; 18.3)*	18.1 (17.7; 18.7)*	219.5 (215.9; 230.8)	0.5 (0.4; 0.5)*	0.7 (0.6; 0.7)*&	4.6 (4.0; 4.7)*	18.1 (15.2; 20.6)*
Group 3 | 3-я группа	9.1 (8.9; 11.2)*	13.3 (8.9; 17.8)*	215.1 (212.7; 219.5)	0.5 (0.4; 0.6)*	0.5 (0.5; 0.6)*	4.6 (4.2; 5.4)*	22.7 (19.8; 22.8)*
Day 14 | 14-е сутки							
Group 1 | 1-я группа	19.9 (18.7; 19.1)*&	20.0 (19.4; 26.8)*	202.4 (184.9; 215.1)	0.56 (0.51; 0.68)*	0.6 (0.5; 0.7)*#&	8.2 (7.5; 8.8)	1.2 (0.9; 1.6)#&
Group 2 | 2-я группа	–	9.6 (9.5; 9.8)*	196.9 (188.9; 209.1)	0.77 (0.61; 0.87)	0.37 (0.35; 0.43)	8.2 (7.3; 8.6)	4.2 (3.8; 4.7)*&
Group 3 | 3-я группа	–	–	198.1 (187.3; 215.7)	0.75 (0.68; 0.77)	0.39 (0.35; 0.40)	7.8 (7.4; 8.3)	8.7 (7.1; 9.9)*

* – significant differences compared with the control group ($p<0.05$) | достоверные отличия с контрольной группой ($p<0,05$)
# – significant differences compared with group 2 ($p<0.05$) | достоверные отличия со 2-й группой ($p<0,05$)
& – significant differences compared with group 3 ($p<0.05$) | достоверные отличия с 3-й группой ($p<0,05$)

in group 1, it demonstrated a 2.5-fold decrease [p=0.0002] (Fig. 2 D) compared with day 3 (Table).

On day 7, in group 1, ultrastructural examination of vessels revealed persistence of the pathological and morphological changes that had been observed on day 3.

In contrast, in groups 2 and 3, we noted a gradual restoration of the endothelial layer of capillaries. Endothelial cells demonstrated a more ordered orientation, and the severity of cytoplasmic edema decreased. However, signs of functional immaturity persisted, including uneven thickness of the endothelial layer, partial disruption of intercellular junctions, and poorly expressed micropinocytotic vesicles and plasmalemmal protrusions (Fig. 3 B).

On day 14, morphologically mature elements of the microcirculatory bed surrounded by well-developed connective tissue were identified in groups 2 and 3 (Fig. 1 E). At the same time, active angiogenesis persisted, as evidenced by a significant increase in VEGF expression, which was 2.8- and 5.8-fold higher in groups 2 and 3 compared with the control group, respectively [p=0.0287; p=0.0001] (Fig. 2 E; Table).

In group 3, the Kernogan index, the pericapillary diffusion index, and arteriolar-venular ratio reached values comparable to those of the control group, indicating restoration of microcirculation in the wound area. In addition, a complete disappearance of altered arterioles and venules was observed in group 3, in contrast to groups 1 and 2. In group 2, despite an overall positive trend, altered venules were still detected, with a numerical density of 9.6 (9.5; 9.8) per 1 mm² of the section. However, this value showed a 1.9-fold decline compared with day 7 (p=0.029) and a 2.1-fold drop compared with group 1 [p=0.017] (Table).

Ultrastructural examination of groups 2 and 3 revealed numerous micropinocytotic vesicles and plasmalemmal protrusions in capillary endothelial cells, along with dense intercellular junctions and a well-formed basement membrane (Fig. 3 C).

In group 1, despite partial restoration of the pericapillary diffusion index, the Kernogan index remained 1.5-fold higher (p=0.0027), while the arteriolar-venular ratio was 1.3-fold lower (p=0.035) than in the control group. VEGF levels returned to those observed in the control group, representing a 2.8-times reduction compared with group 2 and 5.8-times compared with group 3 [p=0.0287 and p=0.0001, respectively] (Fig. 2 F). Persistent alterations in vessels, including stasis, erythrocyte aggregation, and thrombosis, were still detectable (Fig. 1 F).

Ultrastructural analysis showed that group 1 maintained signs of structural and functional insufficiency. We detected areas of endothelial layer thinning, persisting perivascular edema, partially restored intercellular junctions, and poorly expressed micropinocytotic vesicles and plasmalemmal protrusions (Fig. 3 D). Endothelial cells were arranged in a less orderly manner compared with groups 2 and 3.

Discussion

The morphological changes of the microcirculatory bed identified on day 3 of experimental modeling of a purulent oral wound reflected typical features of the acute inflammatory phase. This phase was accompanied by arterial spasm, endothelial dysfunction, and aggregation of blood cellular elements, which lead to making some vessels non-functional. Morphometrically, this was manifested by an increase in the numerical density of altered vessels [13]. More pronounced changes were observed in the group with no wound dressing used (group 1), indicating severe hemodynamic disturbances.

An increase in the Kernogan index in all experimental groups reflected a decrease in the patency of arterioles and impairment of arterial blood inflow due to lumen narrowing and vascular wall thickening. All these processes were caused by inflammatory edema, activation of smooth muscle cells, and biological activity of inflammatory mediators [14].

Changes in the venular component of the microcirculation were characterized by an increase in the numerical density of morphologically altered venules and a decrease in the arteriolar-venular ratio, indicating an inflow–outflow imbalance. Due to increased permeability and lower resistance to inflammatory influence, venules were the first to be involved, which led to the development of venous stasis and aggravation of tissue hypoxia in the affected area [15].

The formation of new microcirculatory elements was evidenced by a significant increase in VEGF expression in the cells surrounding the wound defect. This finding coincided with marked cellular infiltration, indicating the activation of angiogenic mechanisms in the presence of inflammation [16]. In addition, a significant decrease in the pericapillary diffusion index across all groups and pathological ultrastructural changes indicated functional immaturity of the capillary bed [17].

On day 7, the observed improvement in the microcirculatory bed organization reflected the transition of the wound healing from the acute inflammatory to the proliferative phase with active angiogenesis [13]. In particular, a significant decrease in the numerical density of altered arterioles and venules per 1 mm² section in group 3 was associated with a reduction in the severity of the inflammatory response, decreased microbial load, and stabilization of endothelial function. Group 1 exhibited persistent marked morphological alterations, namely thrombosis, edema, and an increased Kernogan index, which indicated sustained exposure to inflammatory mediators and impaired recovery of the arterial portion of the microcirculation. A rise in the numerical density of altered arterioles on day 7 in group 1 (29.6 versus 11.93 on day 3) is attributed to secondary deterioration of microcirculation due to persistently high microbial load and transition to chronic inflammation. This is not an artifact, but rather a characteristic feature of an open purulent process without wound dressing [18].

VEGF expression increase in groups 2 and 3 reflected activation of angiogenesis characteristic of the proliferative stage of wound healing; however, ultrastructural signs of functional immaturity of newly formed vessels were still observed. In group 1, a plunge in VEGF expression was detected, which reflected the formation of poorly vascular-

ized connective tissue that would later contribute to cicatrix deformation at the wound site [16].

Complete restoration of the structural and functional organization of the microcirculatory bed in the group 3 by day 14 was due to the combined effect of local antimicrobial control and favorable conditions for reparative tissue regeneration. Local release of the antibacterial agent from the smart membrane reduced microbial contamination, which led to attenuation of the inflammatory response. This, in turn, contributed to stabilized endothelial function, reduced vascular permeability and perivascular edema, thereby promoting the restoration of hemodynamics and vascular patency [17].

Control of the bacterial load in the wound area limited coagulation cascade activation and reduced blood cell adhesion to the endothelium. Subsequently, altered arterioles and venules disappeared completely, and arteriolar-venular ratio was restored. As inflammation subsided, coordinated angiogenesis proceeded under more favorable conditions with a more orderly spatial organization of endothelial cells, a lower incidence of ultrastructural immature capillaries, and restoration of the pericapillary diffusion index. As a result, functionally adequate angiogenesis ensured sufficient perfusion of regenerating tissues, which accelerated the transition of wound healing from the inflammatory to proliferative and remodeling phases [18].

In addition, the presence of a wound dressing itself served as a barrier limiting secondary microbial contamination and mechanical trauma to the wound surface, which maintained stable microenvironmental homeostasis in the defect area, reduced ischemic-hypoxic stress, and contributed to a more coordinated restoration of microvascular network [19]. Thus, by day 14, we observed that the values of almost all investigated parameters in group 2 returned to control values.

An elevated Kernogan index and a reduced pericapillary diffusion index in group 1 on day 14 indicated persistent elevation of vascular tone and structural remodeling of the vascular wall, even when capillary blood flow relatively normalized [14].

The major limitation of our research is a relatively small number of animals per group and time point (n=15 and n=5, respectively). Nevertheless, statistically significant differences were detected, suggesting a large effect size. To increase statistical power, future studies will use larger sample sizes.

Conclusion

Applying the antibacterial piezoelectric polymer smart membrane promoted wound healing by controlling microbial contamination and indirectly restoring the microcirculatory bed through improved endothelial function, hemodynamics, and angiogenic processes. The observed morphological and morphometric changes indicated the formation of a functionally mature vascular network within a shorter timeframe compared with the groups treated without any wound dressing and with the piezoelectric polymer smart membrane without antibacterial agent.

Author contributions
Conceived the study and designed the experiment – S.A. Sagdullaeva, A.D. Koniaeva, E.Yu. Varakuta, E.N. Bolbasov.
Collected the data and performed the analysis – S.A. Sagdullaeva, O.V. Kukartseva, U.V. Chernova.
Data analysis – S.A. Sagdullaeva.
Wrote the paper – A.D. Koniaeva.
Edited the manuscript – E.Yu. Varakuta, E.N. Bolbasov.

Вклад авторов
Концепция и дизайн исследования – С.А. Сагдуллаева, А.Д. Коняева, Е.Ю. Варакута, Е.Н. Больбасов.
Сбор и обработка материала – С.А. Сагдуллаева, О.В. Кукарцева, У.В. Чернова.
Анализ данных – С.А. Сагдуллаева.
Написание текста – А.Д. Коняева.
Редактирование – Е.Ю. Варакута, Е.Н. Больбасов.

Disclosure. The authors declare no conflict of interest.
Конфликт интересов. Авторы заявляют об отсутствии конфликта интересов.

References/Литература

1. *Komilovich MJ.* Purulent-inflammatory diseases of the maxillofacial region in patients with various chronic diseases. Indonesian Journal of Innovation Studies. 2022;18:637. DOI: 10.21070/ijins.v18i.637.
2. *Kamel NA.* Bio-piezoelectricity: fundamentals and applications in tissue engineering and regenerative medicine. Biophys Rev. 2022;14(3):717–33. DOI: 10.1007/s12551-022-00969-z.
3. *Dai J, Shao J, Zhang Y, Hang R, Yao X, Bai L et al.* Piezoelectric dressings for advanced wound healing. J Mater Chem B. 2024;12(8):1973–90. DOI: 10.1039/d3tb02492j.
4. *Das R, Le TT, Schiff B, Chorsi MT, Park J, Lam P et al.* Biodegradable piezoelectric skin-wound scaffold. Biomaterials. 2023;301:122270. DOI: 10.1016/j.biomaterials.2023.122270.
5. *Goonoo N, Gimié F, Ait-Arsa I, Cordonin C, Andries J, Jhurry D et al.* Piezoelectric core-shell PHBV/PDX blend scaffolds for reduced superficial wound contraction and scarless tissue regeneration. Biomater Sci. 2021;9(15):5259–74. DOI: 10.1039/d1bm00379h.
6. *Rashdan HRM, Tolba E, Abdelraof M.* Cotton gauze wound-dressing patches loaded with dapsone derivative and silver nanoparticles for promoting wound healing via antibacterial acceleration function. RSC Adv. 2025;15(56):48156–70. DOI: 10.1039/d5ra04951b.
7. *Koniaeva AD, Varakuta EY, Leiman AE, Bolbasov EN, Stankevich KS.* Restoration of the microvasculature and hemodynamics in the oral mucosa wound defects area with and without a piezoelectric polymer membrane. Clinical and experimental morphology. 2022;11(3):56–66. DOI: 10.31088/CEM2022.11.3.56-66.
8. *Chernova UV, Tran TH, Bolbasov EN.* Piezoelectric properties of polymer composite membranes with antimicrobial properties for oral mucosal regeneration. In: Proceedings of the II International Siberian Chemical Symposium "SCS-2025" (Tomsk, 20-24 Oct 2025). Tomsk: TPU Publ., 2025. P. 291–292 (In Russ.). Available from: http://earchive.tpu.ru/handle/11683/133669 (accessed 17.03.2026).
9. *Scardina GA, Carini F, Noto F, Messina P.* Microcirculation in the healing of surgical wounds in the oral cavity. Int J Oral Maxillofac Surg. 2013;42(1):31–5. DOI: 10.1016/j.ijom.2012.06.008.

10. *Kalalinia F, Taherzadeh Z, Jirofti N, Amiri N, Foroghinia N, Beheshti M et al.* Evaluation of wound healing efficiency of vancomycin-loaded electrospun chitosan/poly ethylene oxide nanofibers in full thickness wound model of rat. Int J Biol Macromol. 2021;177:100–10. DOI: 10.1016/j.ijbiomac.2021.01.209.
11. *Garraud O, Hozzein WN, Badr G.* Wound healing: time to look for intelligent, 'natural' immunological approaches? BMC Immunol. 2017;18(Suppl 1):23. DOI: 10.1186/s12865-017-0207-y.
12. *Abràmoff MD, Magalhães PJ, Ram SJ.* Image processing with ImageJ. Biophotonics International. 2003;11(7):36–42. Available from: https://www.researchgate.net/publication/228334776_Image_Processing_with_ImageJ (accessed 17.03.2026).
13. *Mayrovitz HN, Aoki K.* Microcirculation in wound healing. In: RF Tuma, JW Breslin, S Peirce-Cottler, WL Murfee (eds.). Handbook of microcirculation. Physiology in health and disease. Cham: Springer, 2023. P. 517–551. DOI: 10.1007/978-3-031-99609-2_10.
14. *Zanoli L, Briet M, Empana JP, Cunha PG, Mäki-Petäjä KM, Protogerou AD et al.* Vascular consequences of inflammation: a position statement from the ESH Working Group on Vascular Structure and Function and the ARTERY Society. J Hypertens. 2020;38(9):1682–98. DOI: 10.1097/HJH.0000000000002508.
15. *Pronina OM, Bilash SM, Kobeniak MM, Koptev MM, Pirog-Zakaznikova AV, Onipko VV et al.* Morphometric features of the structural components of the hemomicrocirculatory bed in the perivulnar region of the caecum in wound defect sutured with polyfilament suture material. Wiad Lek. 2021;74(6):1382–88. PMID: 34159924.
16. *Palomeque Chávez JC, McGrath M, O'Connor C, Dervan A, Dixon JE, Kearney CJ et al.* Development of a VEGF-activated scaffold with enhanced angiogenic and neurogenic properties for chronic wound healing applications. Biomater Sci. 2025;13(8):1993–2011. DOI: 10.1039/d4bm01051e.
17. *Peng S, Wang L, Lu Z, Yang X, Lu Y, Wang Z et al.* An injectable conductive multifunctional hydrogel dressing with synergistic antimicrobial, ROS scavenging, and electroactive effects for the combined treatment of chronic diabetic wounds. Biomater Adv. 2026;179:214498. DOI: 10.1016/j.bioadv.2025.214498.
18. *He J, Chen J, Liu T, Qin F, Wei W.* Research progress of multifunctional hydrogels in promoting wound healing of diabetes. Int J Nanomedicine. 2025;20:7549–78. DOI: 10.2147/IJN.S519100.
19. *Huang Y, Song C, He J, Li M.* Research progress in endothelial cell injury and repair. Front Pharmacol. 2022;13:997272. DOI: 10.3389/fphar.2022.997272.

Author information

Sofia A. Sagdullaeva – Teaching Assistant, Human Anatomy Department with a course of Topographic Anatomy and Operative Surgery, Siberian State Medical University.
https://orcid.org/0000-0002-5730-3411

Anastasiia D. Koniaeva – Cand. Sci. (Med.), Associate Professor, Human Anatomy Department with a course of Topographic Anatomy and Operative Surgery, Siberian State Medical University.
https://orcid.org/0000-0002-9708-1948

Elena Yu. Varakuta – Dr. Sci. (Med.), Professor, Head of Human Anatomy Department with a course of Topographic Anatomy and Operative Surgery, Siberian State Medical University.
https://orcid.org/0000-0003-3173-5336

Evgeny N. Bolbasov – Cand. Sci. (Tech.), Head of Shared Access Additive Technology Center, National Research Tomsk Polytechnic University.
https://orcid.org/0000-0002-6113-1835

Ulyana V. Chernova – Engineer, School of Advanced Engineering "Intelligent Energy Systems", National Research Tomsk Polytechnic University.
https://orcid.org/0000-0002-6714-8785

Oksana V. Kukartseva – Engineer, Shared Access Additive Technology Center, National Research Tomsk Polytechnic University.
https://orcid.org/0009-0007-1559-199X

Информация об авторах

Софья Андреевна Сагдуллаева – ассистент кафедры анатомии человека с курсом топографической анатомии и оперативной хирургии СибГМУ.

Анастасия Денисовна Коняева – кандидат медицинских наук, доцент кафедры анатомии человека с курсом топографической анатомии и оперативной хирургии СибГМУ.

Елена Юрьевна Варакута – доктор медицинских наук, профессор, заведующая кафедрой анатомии человека с курсом топографической анатомии и оперативной хирургии СибГМУ.

Евгений Николаевич Больбасов – кандидат технических наук, директор Центра аддитивных технологий общего доступа НИ ТПУ.

Ульяна Вадимовна Чернова – инженер Инженерной школы «Интеллектуальные энергетические системы» НИ ТПУ.

Оксана Васильевна Кукарцева – инженер Центра аддитивных технологий общего доступа НИ ТПУ.